Er3+-doped silica-hafnia films for optical waveguides and spherical resonators

Giancarlo C. Righini, Simone Berneschi, Gualtiero Nunzi Conti, Stefano Pelli, E. Moser, R. Retoux, Patrice Feron, R. R. Gonçalves, G. Speranza, Yoann Jestin, et al.

Er3+-doped silica–hafnia films for optical waveguides and spherical resonators

G.C. Righini [a,b], S. Berneschi [a], G. Nunzi Conti [a,c], S. Pelli [a], E. Moser [d], R. Retoux [e], P. Féron [f], R.R. Gonçalves [g], G. Speranza [h], Y. Jestin [i], M. Ferrari [i], A. Chiasera [i,*], A. Chiappini [i], C. Armellini [i]

[a] CNR-IFAC, Nello Carrara Institute of Applied Physics, Via Madonna del Piano 10, 50019 Sesto Fiorentino, Italy
[b] CNR-DMD, Department of Materials and Devices, Via dei Taurini 19, 00185 Roma, Italy
[c] Centro Enrico Fermi, Complesso del Viminale, 00185 Roma, Italy
[d] Dipartimento di Fisica, Università di Trento and CSMFO Lab., Via Sommarive 14, 38050 Povo-Trento, Italy
[e] Laboratoire CRISMAT, UMR 6508, ENSICAEN, 6 Blvd. Maréchal Juin, 14050 Caen, France
[f] Laboratoire d'optronique (CNRS-UMR 6082-Foton), ENSSAT, 6 rue de kérampont, 22300 Lannion, France
[g] Departamento de Quimica, Universitade de São Paulo, Av. Bandeirantes 3900, Ribeirão Preto, SP, CEP 14040-901, Brazil
[h] Fondazione Bruno Kessler, Via Sommarive 18, 38050 Povo-Trento, Italy
[i] CNR-IFN, Istituto di Fotonica e Nanotecnologie, CSMFO Lab., Via alla Cascata 56/c, 38050 Povo-Trento, TN, Italy

In this paper we present some result on sol–gel derived silica–hafnia systems. In particular we focus on fabrication, morphological and spectroscopic assessment of Er^{3+}-activated thin films. Two examples of silica–hafnia-derived waveguiding glass ceramics, prepared by top–down and bottom–up techniques are reported, and the main optical properties are discussed. Finally, some properties of activated micro-spherical resonators, having a silica core, obtained by melting the end of a telecom fiber, coated with an Er^{3+}-doped $70SiO_2$–$30HfO_2$ film, are presented.

1. Introduction

Since the discovery of optical fibers, the possibility to develop optically confined structures has opened new possibilities for making novel optical components [1]. Rare earth-activated confined structures offer thus interesting solutions for this end. The growing activity in this field is aimed to the development of optical amplifiers in planar form based on rare-earth-activated glasses to provide devices such as lossless splitters, which can find applications in the metropolitan and local area networks [2]. Since the pioneer work of 1993, when Wang and Ohwaki discovered novel glass–ceramic system characterized by a transparency comparable to a glass [3], considerable efforts have been made in order to fabricate rare earth activated glass–ceramic materials with active ions embedded in the crystalline phase [4]. The motivation for this research is combining the mechanical and optical properties of the glass with a crystal-like environment for the rare-earth ions, where their higher cross-sections can be exploited in order to fabricate more compact devices [5,6]. Moreover, ceramic glasses materials may be a valid alternative method to control chemical parameters of the rare earth, and thus may avoid undesirable effect like

* Corresponding author. Tel.: +390461314923; fax: +390461881696.
E-mail address: achiaser@science.unitn.it (A. Chiasera).

clustering as proposed by Auzel and Goldner [7]. It should be mentioned that these nanocomposite systems are of particular interest for photonic application when the glass ceramics can be prepared in waveguiding configuration as recently reported by Jestin et al. that have shown that SiO_2–HfO_2: Er^{3+} glass–ceramic planar waveguides prepared by sol–gel route present valuable optical, spectroscopic and structural features for successful applications in the telecommunication area [8,9]. A further development in the control of luminescence properties can be achieved by rare earth-activated microcavities, which represent a particular class of photonic crystals, as well as spherical microresonators where light can be guided in dielectric spheres through high-Q whispering-gallery-modes (WGMs). A unique combination of strong temporal and spatial confinement of light can be achieved in such structures: this makes microspheres very interesting for a large number of applications as diverse as cavity quantum electrodynamics, nonlinear optics, photonics, and chemical/biological sensing [10].

Although these systems can be prepared by several techniques the always-growing number of papers devoted to sol–gel-based photonics materials and devices, is the better demonstration that sol–gel process is a useful method for fabrication of optoelectronic components and their integration. Among the several binary systems, which are possible to prepare by sol–gel route, the SiO_2–HfO_2 binary system has demonstrated to be really efficient for successful applications in photonics [11]. In fact, not only the preparation is simple and samples with high reproducibility can be prepared with a suitable protocol, but also refractive index can be tailored as a function of the composition and phase separation can be controlled by the HfO_2 concentration and the annealing procedure.

The aim of this paper is to give a short review of the use of SiO_2–HfO_2 in the following glass-based photonic systems: (i) rare earth-activated glass ceramics planar waveguides, where the active ions are embedded in the crystalline phase, combining the mechanical and optical properties of the glass with a crystal-like environment for the rare-earth ions; (ii) microspheres prepared by fusion of a standard telecom fiber and coated by a $70SiO_2$–$30HfO_2$ film activated by Er^{3+} ions. Optical and spectroscopic assessment, as well as morphological and structural characterization of these systems is reported.

2. Erbium-activated silica–hafnia amorphous planar waveguides

Eight $70SiO_2$–$30HfO_2$ planar waveguides activated by different molar percentages of erbium ion were prepared by sol–gel route using the dip-coating technique [11,12]. The waveguides were prepared using the sol–gel method and dip-coating technique. The starting solution, obtained by mixing tetraethylorthosilicate (TEOS), ethanol, deionised water and hydrochloric acid as a catalyst, was pre-hydrolysed for 1 h at 65 °C. The molar ratio of TEOS:HCl:EtOH:H_2O was 1:0.01:37.9:2. An ethanolic colloidal suspension was prepared using as a precursor $HfOCl_2$ and then added to the TEOS solutions, with a Si/Hf molar ratio of 70/30. Erbium was added as $Er(NO_3)_3{\cdot}5H_2O$ with a Er/(Si + Hf) molar concentration ranging from 0.01 to 4 mol%. The final mixture was left at room temperature under stirring for 16 h. The obtained sol was filtered with a 0.2 μm Millipore filter.

Erbium-doped silica–hafnia films were deposited on cleaned pure v-SiO_2 substrates by dip-coating, with a dipping rate of 40 mm/min. Before further coating, each layer was annealed in air for 50 s at 900 °C. After a 10 dipping cycle, the film was heated for 2 min at 900 °C. Final films, resulting from 20 or 25 coatings, were stabilized by the last treatment for 5 min in air at 900 °C. As a result of the procedure, transparent and crack-free waveguides were obtained. The thickness of the waveguide and the refractive index at 543.5 and 632.8 were measured in TE and TM polarizations, by an m-line apparatus [11].

The waveguides presented thickness ranging from 0.6 to 1.0 μm, and a refractive index of 1.61 ± 0.01 measured at 632.8 nm in the TE polarization. For all samples and both at 632.8 and 543.5 nm the refractive index measured in TE polarization is higher ($\Delta n = 0.013 \pm 0.002$) than in TM polarization, indicating that birefringence is not negligible in our system.

The TE_0 mode excitation was used for photoluminescence (PL) measurements, detecting the scattered light from the front face of the waveguide. The PL spectroscopy, in the region of the $^4I_{13/2} \rightarrow {}^4I_{15/2}$ transition of Er^{3+} ions, was performed using the 980 nm emission of a Ti:sapphire laser. The details about the experimental setup were previously reported [11].

The more significant spectroscopic parameters of the waveguides are reported in Table 1. A spectral bandwidth of 48 nm, measured at 3 dB from the maximum of the 1533 nm emission was observed in all waveguides. The fact that both shape and FWHM of the $^4I_{13/2} \rightarrow {}^4I_{15/2}$ transition are independent on erbium content is related to the specific properties of Hf^{4+} on the glass network. Hf^{4+} increases the number of Si–O non-bridging groups [13] accounting for a general network flexibility, which may conceivably accommodate Er^{3+} contents without appreciable matrix strains.

The active ions concentration is a critical parameter to design planar waveguides for photonics applications. In fact, when the erbium concentration increases, other problems become important. The average distance between neighboring erbium ions decreases, and electric dipole–dipole interactions between the different erbium ions become more significant.

Under this condition, processes including energy migration and upconversion can take place, lowering the fraction of excited Er^{3+} at a given pump power [14]. As a consequence, a decrease of the luminescence lifetime of the metastable $4I_{13/2}$ state as a function of the increasing Er^{3+} concentration occurs, as described in the following empirical formula [15]:

$$\tau_{obs} = \frac{\tau_0}{1 + \left(\frac{r}{Q}\right)^p}, \quad (1)$$

where τ_{obs} is the observed luminescence lifetime, τ_0 the ideal luminescence lifetime in the limit of zero concentration, r is the Er^{3+} ion concentration, Q is the quenching concentration and p a phenomenological parameter characterizing the steepness of the corresponding quenching curve. By fitting the experimental data of Table 1 with the empirical formula (1) we have obtained the following parameters: $\tau_0 = 6.8$ ms, $Q = 0.81$ mol% and $p = 1.3$. Finally, we note that for all the waveguides the $^4I_{13/2}$ level decay curves presented a single-exponential profile. As an example, Fig. 1 shows the normal-

Table 1
Spectroscopic parameters characterizing the $70SiO_2$–$30HfO_2$ planar waveguides activated by different Er/(Si + Hf) mol% content. Decay time constants of the $^4I_{13/2}$ level of Er^{3+} ions and FWHM spectral bandwidth of the $^4I_{13/2} \rightarrow {}^4I_{15/2}$ transition are reported. Measurements were performed at room temperature upon 980 nm excitation.

Waveguides	Er^{3+} (mol%)	FWHM (±2 nm)	Lifetime (±0.5 ms)
SH001	0.01	48	6.7
SH003	0.03	48	6.5
SH01	0.1	48	6.5
SH03	0.3	48	5.0
SH05	0.5	48	4.2
SH1	1.0	48	2.9
SH2	2.0	48	1.8
SH4	4.0	48	1.8

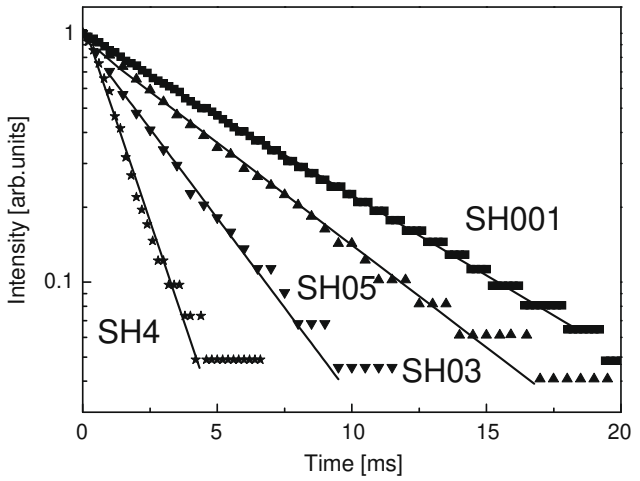

Fig. 1. Room temperature decay curves of the luminescence from the $^4I_{13/2}$ metastable state of Er^{3+} ions for the $70SiO_2$–$30HfO_2$ planar waveguide doped with 0.01 (SH001), 0.03 (SH03), 0.5 (SH05), and 4 (SH4) Er/(Si + Hf) mol%. Measurements were performed upon excitation at 980 nm. The solid lines represent single exponential fits to the decay data.

ized decay curves of the $^4I_{13/2}$ state for some silica–hafnia waveguides. The measured lifetime of 6.7 ms, which characterize the SH001 waveguide, can be assumed very close to the radiative lifetime of the $^4I_{13/2}$ metastable level of Er^{3+} ion in $70SiO_2$–$30HfO_2$ glass since at this low concentration no interaction between Er^{3+} ions occurs. It is worthy of note that the quenching concentration effect and correlated energy transfer processes appear negligible in $70SiO_2$–$30HfO_2$ waveguides, for Er^{3+} concentration up to 0.1 mol% (see Table 1 and Fig. 1) indicating the high quantum efficiency of the $^4I_{13/2}$ state in this system.

The Raman spectrum reported in Fig. 2 gives further information about the useful properties of the SiO_2–HfO_2 binary system. The Raman spectrum of the v-SiO_2 is also reported for comparison. Raman spectra were collected in the VV polarization, by exciting the TE_0 mode with an Ar^+ ion laser.

As observed comparing the Raman spectrum of the silica–hafnia waveguides SH03 with that of the fused silica, the presence of hafnium oxide promotes a strong modification of the silica structure. The appearance of the 970 cm^{-1} Raman band suggests the effective

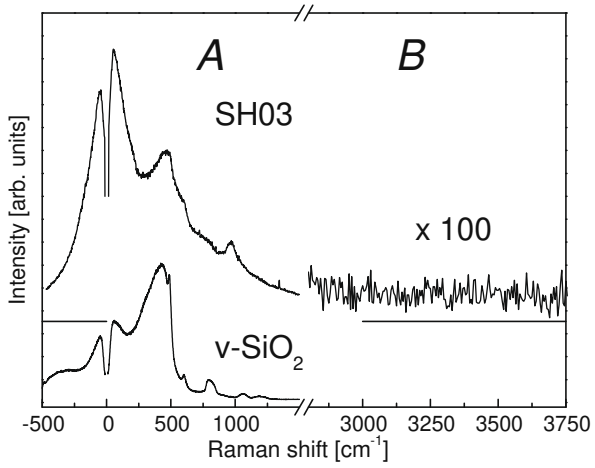

Fig. 2. Room temperature Raman spectra of the SH03 $70SiO_2$–$30HfO_2$ planar waveguide collected in VV polarization with excitation of the TE_0 mode at 457.9 nm (A) and 514.5 nm (B). Raman spectrum of the v-SiO_2 is also reported for comparison.

molecular mingling of SiO_2–HfO_2 components of the films [13]. A complete densification is achieved for all samples. In fact, the bands characteristic of the OH groups in silicate glasses, generally observable at 3670 and 3750 cm^{-1}, are absent in the portion of the Raman spectra shown with a magnification of 100 [16]. The Raman spectra do not show any evidence of hafnia crystallization, that would display several sharp peaks in the region between 100 and 800 cm^{-1} [17].

A $70SiO_2$–$30HfO_2$ mol% planar waveguide activated with 0.3 mol% of Er^{3+}, deposited on silica-on-silicon (SoS) substrate, was prepared by using sol–gel route and dip-coating technique. We have chosen this erbium concentration in order to have the best compromise between signal intensity and lifetimes. The waveguide shows thickness of 1.0 μm, and a refractive index of 1.60 at 632.8 nm, supporting a well confined single propagation mode at 1.5 μm (confinement coefficient of 0.85).

An attenuation coefficient of 0.8 dB/cm at 632.8 nm was measured. A lifetime of 5.9 ms for the $^4I_{13/2}$ metastable state of the Er^{3+} ions was measured. The spectral bandwidth at 1.53 μm, measured at 3 dB from the maximum of the intensity, was of about 44 nm. We have prepared channel waveguides by using a dry-etching process on this planar waveguide.

3. Silica–hafnia-derived waveguiding glass ceramics prepared by top–down technique

Er^{3+}-doped silica–hafnia planar waveguides were fabricated by sol–gel technique. The erbium content was 1 mol% for a silica hafnia ratio of 70:30. We use the fabrication protocol described above to deposit the starting amorphous waveguides. Nanocrystals were obtained with an additional heat treatment in air at temperature between 1000 °C and 1100 °C for 30 min in order to investigate more precisely the effect of crystallization on spectroscopic properties. The samples were introduced in the furnace at the temperature of 800 °C with a heating rate of 15 °C/min in order to avoid surface cracking. The thermal treatments of each glass–ceramics samples are summarized in Table 2 [18,19].

The waveguides presents a thickness from 0.3 to 0.6 μm and a refractive index close to 1.61 measured at 632.8 nm in the TE polarization. All waveguides support at least one TE mode at 1.5 μm. For all the samples, the refractive index measured at 632.8 nm, 543 nm, 1319 nm and 1542 nm in TE polarization is higher than in TM polarization, indicating that birefringence is not negligible in the system. The waveguides W900 and W1000 were prepared following the same protocol and they differed from one another only in the thermal treatments. The losses observed for the samples W900 and W1000 are respectively 0.7 and 1 dB/cm: this makes them suitable for operation in the C telecommunication band. The increase of losses is due to the scattering induced by the nanocrystals. The relatively high propagation losses observed for the sample W1100 are due to a larger size of the nano-

Table 2
Annealing temperature, size of nanocrystals, attenuation coefficient, and $^4I_{13/2}$ lifetime of the Er^{3+}-activated SiO_2–HfO_2 planar waveguides [18,19].

Waveguide labeling	W900	W1000	W1100
Thermal treatment (°C)	900	1000	1100
Number of dips	20	20	30
Crystallite size (nm)	–	3	5
Number of mode@1542	1	1	2
Thickness (±0.1 μm)	≅0.3	≅0.3	0.6
Attenuation coefficient@1542 nm (±0.3 dB/cm)	0.7	1.0	⩾2
Lifetime@1542 nm (±0.5 ms)	2.0	5.1	6.1
FWHM (nm) (±0.2 nm)	48	21	20

crystals but also to the surface degradation caused by the high temperature thermal treatment.

The average of the crystallite size obtained by X-ray diffraction are summarized in Table 2 as a function of the heat treatment. The size of the crystallites becomes more important with the thermal treatment, from 3 nm for the sample W1000 to 5 nm for the sample W1100. Higher temperature and longer annealing times cause an increase in the average crystallite size. An important requirement for ultra-transparent glass ceramics fabrication is that the crystallites should be sufficiently small to keep Rayleigh scattering losses to an acceptable low level. This seems to be the present case. In fact, the waveguide heat-treated at 1000 °C shows good propagation properties at 1.5 μm with losses around 1 dB/cm, which thus make it a suitable component for low losses amplifier in the C band of telecommunication. Further information about the structural properties of the waveguides were obtained by Raman measurements. Fig. 3 shows the Raman spectra of W1000 and W1100 samples collected in VV polarization using the 457.9 nm line of a CW Argon-laser as excitation source. Those ones are compared to the W900 sample heat treated at 900 °C. The heat treatment promote a strong modification in the spectra and in particular a crystallization process, evidenced by (i) the structures in the region between 100 and 1000 cm^{-1} attributed to HfO_2 crystals vibrations; (ii) the decrease of the intensity of the band at about 970 cm^{-1} attributed to the Si–O–Hf stretching [11]; (iii) the presence of a band centred at about 310 cm^{-1}, which is assigned to the Hf–O–Hf vibrations [20]; (iv) the presence of intense sharp band in the low frequency region, indicating the presence of nanocrystals. This band shifts toward low frequency with the annealing temperature. We attribute these bands to acoustic vibrations of the HfO_2 nanocrystals. Their position in the spectra is proportional to the inverse of the particle diameter [21].

Fig. 4 show the room photoluminescence spectra of erbium doped SiO_2–HfO_2 planar waveguides, as a function of the heat treatment. For precursor waveguide, as well as for glass–ceramics planar waveguides, luminescence from the excited $^4I_{13/2}$ state is observed, with a main emission peak at 1532 nm. The shape of the luminescence spectra, relative to the $^4I_{13/2} \rightarrow {}^4I_{15/2}$ in the 1.5 μm region, is very sensitive to the local environment of the rare earth ion. The modifications of the spectra confirm the significant modification of erbium ions environment in glass–ceramics systems. The order of the crystal-like local environment, limits the inhomogeneous broadening typical of glassy environment and, therefore, the bandwidth decreases from 48 nm to 21 nm and

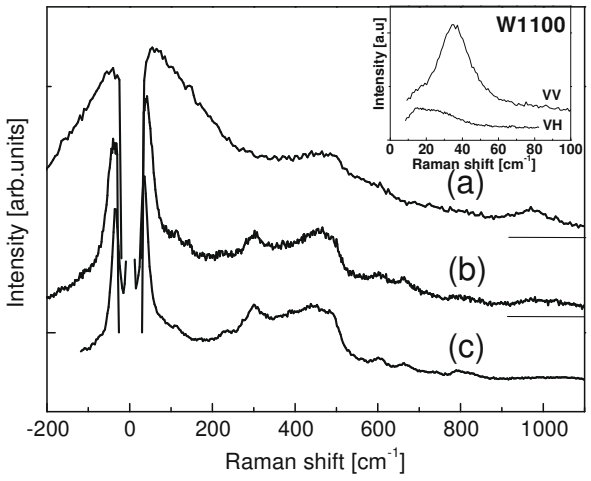

Fig. 3. Raman spectra of (a) W900, (b) W1000, (c) W1100 planar waveguides, collected in VV polarization with excitation of the TE_0 mode at 457.9 nm [19].

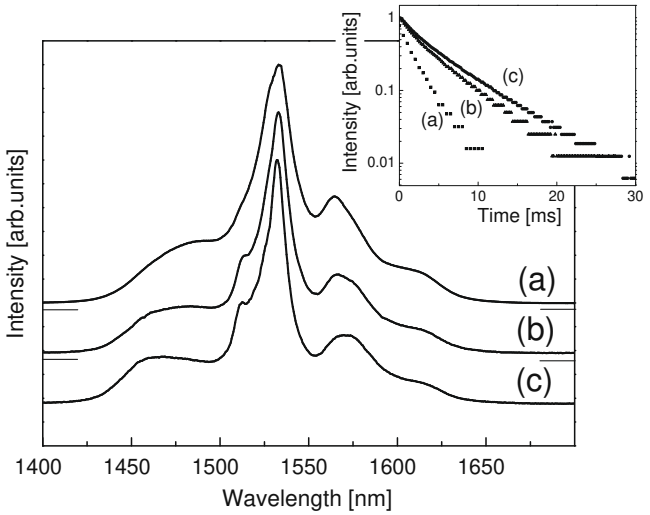

Fig. 4. Room temperature luminescence spectra of the $^4I_{13/2} \rightarrow {}^4I_{15/2}$ transition of Er^{3+} ion for the (a) W900, (b) W1000, (c) W1100 planar waveguides, obtained by exciting the TE_0 mode at 514.5 nm. In the inset are reported the decay curves of the luminescence from the $^4I_{13/2} \rightarrow {}^4I_{15/2}$ metastable state of Er^{3+} ions for the respective samples upon 514.5 nm excitation [18,19].

20 nm for the waveguides W900, W1000 and W1100, respectively. The $^4I_{13/2} \rightarrow {}^4I_{15/2}$ emission band of the glass–ceramics presents well-resolved Stark components in agreement with a crystalline-like environment for the Er^{3+} ion [18,19].

The shape and the bandwidth of the emission spectra do not change with the excitation wavelength, i.e. 980 nm and 514.5 nm, indicating that site selection is negligible.

The lifetime of the metastable level $^4I_{13/2}$ have been measured at 1532 nm for the different samples. The decay curves are shown in the inset of Fig. 4. According to the decay curves measured for the $^4I_{13/2}$ emission upon 514.5 nm excitation, the lifetime of the emission increases with the increase of the heat-treatment temperature, from 2.0 ms for the precursor waveguide, to 5.1 ms for the waveguide glass ceramic W1000 heat treated at 1000 °C, and 6.1 ms for the waveguide glass ceramic W1100 heat treated at 1100 °C. This behavior clearly demonstrate that Er^{3+} ions are embedded in nanocrystals. The decay curves cannot be fitted by a single exponential function, which probably means that the erbium ions are not feeling the same local environment. By fitting the decay curves with two different single exponential, we can notice two different parts: one part corresponding at the erbium ions in the glass matrix leading to a lifetime close to 2.0 ms, and the second part corresponding to erbium ions embedded in the crystalline environment leading to a lifetime close to 7.0 ms. It's important to note that the embedding of erbium ions in the HfO_2 crystalline phase induces an important enhancement of the lifetime of the metastable level $^4I_{13/2}$.

4. Silica–hafnia-derived waveguiding glass ceramics prepared by bottom–up technique

Using a bottom–up approach SiO_2–HfO_2:Er^{3+} glass–ceramic planar waveguides were realized by following the described protocol [9]: (1) preparation of a colloidal suspension of HfO_2 nanoparticles, starting from a $HfOCl_2$ solution in ethanol and using a reflux technique. (2) Separation of HfO_2 nanoparticles from the colloidal suspension. (3) Preparation of a solution of TEOS, alcohol, deionised water and hydrochloridric acid prehydrolized for 1 h at 65 °C, in which has been added the hafnia precursor $HfOCl_2$ in order to obtain a final solution with a molar ration Si/Hf = 80/20. (4) At this

solution has been added $Er(NO_3)_3{\cdot}5H_2O$ with a molar concentration Er/(Si + Hf) = 1, and hafnia nanoparticles in order to have 2.5 mol% of nanoparticles in the solution. Nanocomposite planar waveguides were produced by dip-coating the final solution on SiO_2 substrate and were stabilized by a thermal treatment at 900 °C in air for 22 h (see Table 3).

After introduction of hafnia nanoparticles, in the silica–hafnia sol, a HRTEM image of the produced waveguide has been performed as shown in Fig. 5. Nanocrystals of about 3–4 nm in size are visible and homogeneously dispersed in the amorphous matrix. Thus confirming the feasibility of the bottom–up approach for the production of nanocomposite waveguides. The EDS analysis has confirmed that the nanocrystals are composed by hafnium oxide.

Fig. 6 compares the $^4I_{13/2} \rightarrow {}^4I_{15/2}$ photoluminescence spectrum of the nanocomposite waveguide (W1) activated by Er^{3+} ions, and the PL spectrum of a silica–hafnia: Er^{3+} waveguide without nanocrystals (W2). As previously seen on the top–down prepared samples, the modification of the emission spectrum of W1 is attributed to the presence of hafnia nanocrystals. The ordering of the local environment limit the inhomogeneous broadening typical of glassy structural environments and therefore the FWHM become smaller from 45 nm to 27 nm for W2 and W1 respectively. We can consider that the thermal treatment at 900 °C which does not damage the surface of the film, promote the migration of erbium ions toward hafnia nanocrystals [22].

The lifetime of the metastable level $^4I_{13/2}$ has been measured at 1532 nm. The decay curves present a single exponential behavior and show that the lifetime of the emission increases for the sample W1 containing nanocrystals, from 4.5 ms for the sample W2, to 5.6 ms for the W1. So the same behavior is observed for the so called bottom–up samples and the top–down samples, indicating that for the bottom–up sample simple a thermal treatment at 900 °C is necessary to promote the migration of erbium ions toward hafnia nanocrystals.

Table 3
Annealing temperature, size of nanocrystals, attenuation coefficient, and $^4I_{13/2}$ lifetime of the Er^{3+}-activated SiO_2–HfO_2 planar waveguides.

Waveguide labeling	W1	W2
Thermal treatment (°C)	900	900
Crystallites size (±1 nm)	3–4	0
Losses@1542 nm (±0.3 dB/cm)	0.3	<0.3
Lifetime@1532 nm (ms)	5.6	4.5

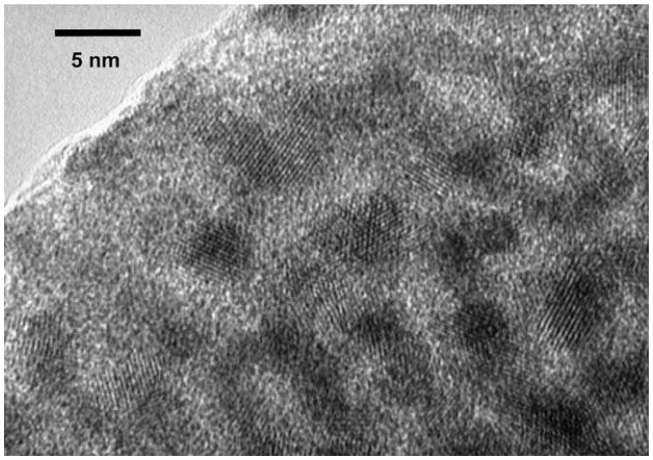

Fig. 5. HRTEM image of the glass–ceramic waveguide W1 showing HfO_2 nanocrystals dispersed in the amorphous matrix.

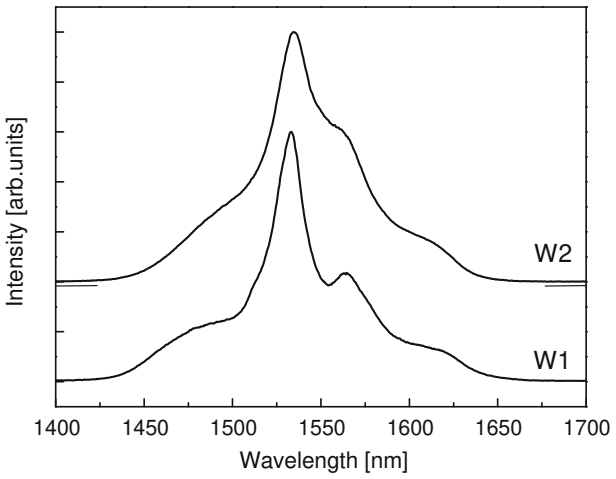

Fig. 6. Room temperature luminescence spectra of the $^4I_{13/2} \rightarrow {}^4I_{15/2}$ transition of Er^{3+} ion for the for the W1, W2 planar waveguides, obtained by exciting the TE_0 mode at 514.5 nm.

The bottom up waveguide W1 presents excellent propagation properties at 1.5 μm with losses around 0.3 dB/cm which thus make it a suitable component for low losses amplifier in the C band of telecommunication [9,23].

It's important to note how the bottom–up method permits to ameliorate the optical properties of the glass–ceramic waveguide with respect to the ones obtained by the top–down method. The top–down method requiring a high thermal treatment at 1000 °C, to grow nanocrystals in the matrix, induces optical losses of 1 dB/cm at 1542 nm, caused by a degradation of the waveguide surface [9].

5. Activated microspherical resonators

Silica is an important material for the preparation of microsphere due to the low losses observed at the telecom wavelength and in particular at 1.55 μm. In our case, silica microspheres serving as a base resonator structure were made by melting the end of a stripped standard telecommunication fiber (SMF 28). After melting and solidification controlled by surface tension, a near-perfect spherical shape, with a radius of thousand of micrometer was achieved.

In order to funzionalize the surface, a thin film has been deposited using a sol–gel method. For the deposition of the active coating of the microspheres we use the fabrication protocol develop for the deposition of the silica–hafnia amorphous planar waveguides. The erbium content has been fixed to 0.1 mol% and 1 mol% for a silica hafnia ratio of 70:30. As a result of these procedures, crack free films surrounding microspheres were obtained. The main characteristics of the microspheres are summarized in Table 4.

Photoluminescence measurements in the region of the $^4I_{13/2} \rightarrow {}^4I_{15/2}$ transition of the Er^{3+} ions were performed using the 514.5 line of an Ar^+ laser as excitation source, detecting the scattered light from the microsphere in free space configuration and dispersing the luminescence light with a 320 mm single grating.

Table 4
Physical characteristics of the microresonators.

Microsphere	Base sphere diameter (μm ± 5 μm)	Erbium content (mol%)	Thickness estimation of the active film (μm)	Refractive index
M1	250	1	0.8	1.53
M2	430	0.1	1.1	1.56

The light was detected using a InGaAs photodiode and a lock-in technique. Decay curves were obtained by chopping the CW exciting beam with a mechanical chopper and recording the signal with a digital oscilloscope. All the measurements were performed at room temperature [9,18,19].

To excite High-Q WGMs (lowest n which correspond to the lowest value of the radial order), light has to be launched from a phase-matched evanescent wave in an adjacent waveguide or a prism under total internal reflection. For microspherical lasers, most of couplings have been realized by prisms [24], tapers [25,26] and half tapers [27]. Among the different pumping wavelengths which can be used with Erbium doped glasses (810 nm, 975 mm and 1480 mm) we chose 1480 nm to obtain a good overlap between the pump and laser mode volumes in the micro-sphere and to optimize the lasing process in our system. Another advantage of using one single tapered-fiber is that the pump wavelength is close enough to that of the laser field, so both pump and laser fields can be coupled in and out the microsphere. The fiber coupling experiments were performed with a tapered fiber, that we obtained by heating and stretching standard telecommunication fiber (single mode at 1.55 μm). Further details on the experimental setup can be found in Ref. [28].

Fig. 7 represents the SEM image of a previous microsphere prepared to have an estimation of the rugosity of the deposited film with a diameter of about 200 μm after the dip coating, and also a part of the fiber, also permitting to estimate the thickness of the deposited film (0.8 μm). We can notice here the good quality of the coating. The observed defects are due to the silica based microsphere used as substrate.

In our case the quality factor Q could be limited by the quality factor of the surface of the sphere, which, for the mode with generic radial order n at the wavelength λ, is given by the Eq. (2) [29]:

$$Q_{\text{surf}} = (3\lambda^2 d^{10/3})/(16\pi^5\sigma^2 Ns^2 n^{5/2}), \tag{2}$$

where σ is the roughness, Ns is the refractive index of the sphere, and d is the sphere diameter. In our case a low roughness σ inferior to 1 nm has been measured, thus indicating that the global quality factor won't be limited by the surface quality of the coating.

The PL spectra relative to the ${}^4I_{13/2} \rightarrow {}^4I_{15/2}$ transition of the Erbium ions obtained upon excitation at 514 nm for M1 and M2 microresonator exhibits a main emission peak at 1.53 μm with a shoulder at about 1.55 μm and a spectral bandwidth of about 48 nm, measured at 3 dB from the maximum of the intensity. Upon excitation at 980 nm, it has been seen that the shape and the bandwidth of the emission spectra do not change with the excitation wavelength, indicating negligible site selection for erbium ions. The PL spectra are quite similar, according to a constant site-to-site inhomogeneity. The decay curves have a single exponential behavior with a lifetime of 4.4 ms and 6.2 ms is respectively obtained for the microsphere doped with 1 mol% and 0.1 mol%. The same lifetimes were measured upon 980 nm excitation. The decrease of the lifetime with the increase of the erbium concentration suggests that energy transfer processes, including cross-relaxation and up-conversion, are effective. In fact, infrared-to-green up-conversion upon 987 nm excitation is observed in the most concentrated microresonator M1 (1 mol%), green emission being visible with the naked eye.

Fig. 8(A) represent the fluorescence spectra of the microsphere M1 after excitation of the whispering gallery modes by a fiber taper as function of the intensity of the pump injected in the sphere.

In microspherical resonator the high energy concentration in whispering gallery modes generally leads to a dependence in wavelength of the emission spectra in function of the temperature, as described by the Eq. (3) [30]:

$$\Delta\lambda = \lambda\left(\frac{1}{Ns}\frac{\partial Ns}{\partial T} + \frac{1}{d}\frac{\partial d}{\partial T}\right)\Delta T. \tag{3}$$

With Ns the refractive index of the material, T the temperature, and d the sphere diameter.

As the temperature inside the spherical resonator is directly linked to the pump power at 1480 nm injected in the sphere, we can expect for a shift towards high wavelengths. In our case, sol–gel coating of silica hafnia seems to be quasi independent with this behavior due to thermal effect linked to the injected pump, in the studied pump power range i.e. tens of mW. We can notice that a very low red shift is observed in this case, and must be typical of the glass system silica hafnia. By comparison with other glass system presented in the literature [31–33].

The measured spectra of M2 presented in Fig. 8(B) put in evidence the two polarization TE and TM for the mode $n = 1$. It's important to remind that the indices l (orbital), n (radial), and m (azimutal) permit to write the energy repartition in whispering gallery modes, using the following expressions (4) [29]:

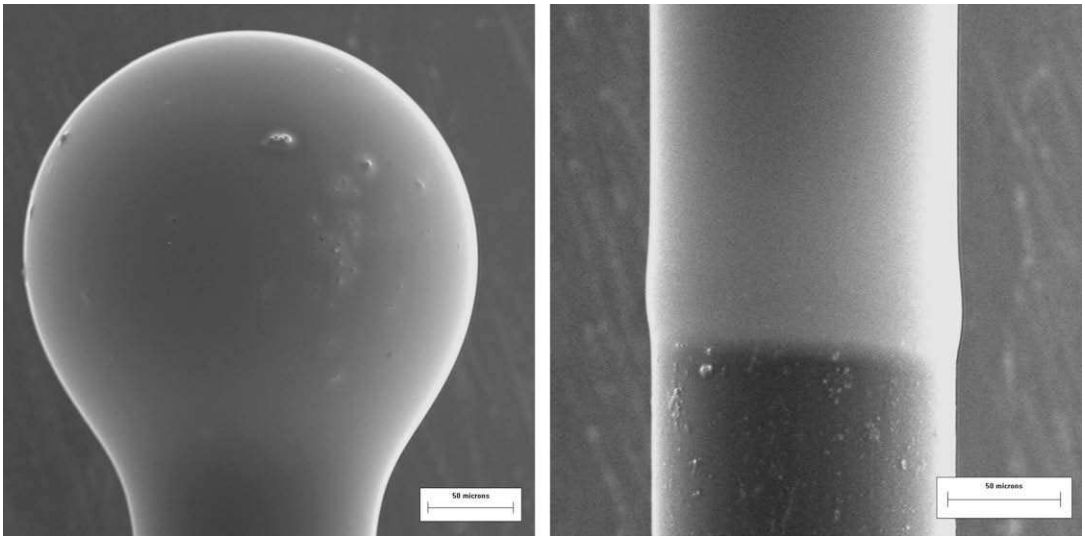

Fig. 7. Silica based microsphere coated with a SiO_2/HfO_2 thin film and activated with erbium ions (left). Coated fiber permitting to estimate the thickness of the deposited film (right).

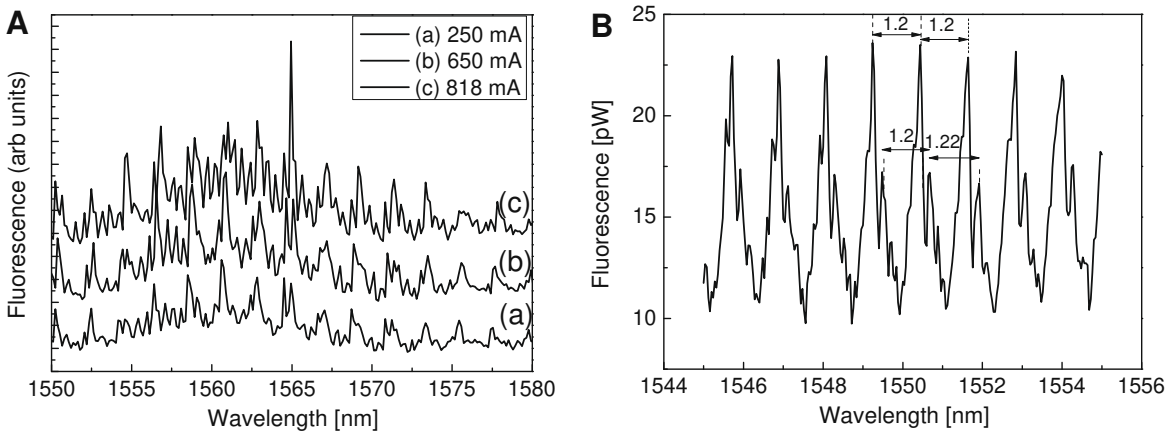

Fig. 8. (A) Fluorescence spectra for M1 microsphere; (B) fluorescence spectra measured for M2 microsphere, indicating the FSR of the microsphere.

$$\Delta\lambda_{n,l} = \frac{\lambda^2}{\pi Nsd}, \quad \Delta\lambda_{n,l}^{\mathrm{TE,TM}} = \frac{\lambda^2}{\pi Nsd} * \frac{\sqrt{Ns^2 - 1}}{Ns}. \tag{4}$$

Thus we can deduce the sphere diameter d. In the present case $d = 430 \pm 10$ μm and the refractive index is $Ns = 1.56$.

By looking closer at the emission spectra of this sphere we can notice a degenerating effect of m. We estimate at 4 the maximal value of $|l - m|$, the azimuthal index. This degenerating effect find certainly his origin in the ellipticity presented by the sphere after the coating. By measuring the spectral difference in wavelength between the two values of m, we can deduce the ellipticity of the sphere. We have to note that in the used configuration we measure the $m > 0$. In fact we have [34]:

$$\Delta\lambda_{n,l,m}^{\Delta m=1} = e * \mathrm{FSR}_{\lambda}, \quad e = \frac{r_p - r_e}{a}. \tag{5}$$

With r_e as the equatorial, r_p the polar, and a the equivalent radii of the sphere.

Using $\Delta\lambda = 0.15058$ nm, we find an ellipticity of 0.12%. This ellipticity due to an inhomogeneous thickness of the coating of the sphere also brings a lot of losses characterized on the spectra by too important full width at half maximum for this kind of microresonator. In this kind of configuration we usually obtain quality factors Q of 10^6.

6. Conclusions

This paper is to give a short review of the use of SiO_2–HfO_2 in various glass-based photonic systems. In particular we have showed that Er^{3+}-activated $70SiO_2$–$30HFO_2$ planar waveguides with valuable optical and spectroscopic properties can be prepared by the sol–gel technique. A full densification can be achieved without crystallization, the quenching concentration effect and correlated energy transfer processes appear negligible in $70SiO_2$–$30HfO_2$ waveguides, for Er^{3+} concentration up to 0.1 mol% indicating the high quantum efficiency of the $^4I_{13/2}$ state in this system. Moreover nanostructured silica based glass–ceramic composite material in which the crystalline nanophase can behave as a suitable host for the luminescence rare earth ions have been fabricated from and Er^{3+} activated $70SiO_2$–$30HfO_2$ planar waveguide prepared by the sol–gel technique with dip coating processing thus becoming successful for EDWA applications. A fabrication procedure based on the top–down approach was defined and an attenuation coefficient of 1 dB/cm was measured at 1542 nm of the sample with crystallites of a mean size of 3 nm. A bottom–up approach was also employed and we have demonstrated how it permit to fabricate silica–hafnia-derived waveguiding glass ceramics with an attenuation coefficient of 0.3 dB/cm at 1542 nm and with crystallites of a mean size of 3–4 nm.

A set of microspheres prepared by fusion of a standard telecom fiber were coated by a $70SiO_2$–$30HfO_2$ film activated by Er^{3+} ions. It is shown how this special geometry can allow the tailoring of the whispering gallery modes thus permitting to select the radial order n of the active whispering galley modes. Furthermore this very cheap protocol and simple method leads to very low roughness surfaces. The quasi independent behavior due to thermal effect linked to the injected pump also brings a major interest for lasing applications.

Acknowledgements

Authors acknowledge the partial financial support of CNR-CNRS (2004–2007), IT-VIET Executive Programme 2006–2008, COST action MP0702, Galileo project 2007 and ITPAR (2008–2011) projects.

References

[1] E.J. Murphy (Ed.), Integrated Optical Circuits and Components, Design and Applications, Marcel Dekker Inc., New York, 2000.
[2] G.C. Righini, S. Pelli, M. Ferrari, C. Armellini, L. Zampedri, C. Tosello, S. Ronchin, R. Rolli, E. Moser, M. Montagna, A. Chiasera, S.J.L. Ribeiro, Opt. Quant. Electron. 34 (2002) 1151.
[3] Y. Wang, J. Ohwaki, Appl. Phys. Lett. 63 (1993) 3268.
[4] M.C. Gonçalves, L.F. Santos, R.M. Almeida, C.R. Chimie 5 (2002) 845.
[5] M. Mortier, F. Auzel, J. Non-Cryst. Solids 256&257 (1999) 361.
[6] M. Mortier, Phil. Mag. B 82 (2002) 745.
[7] F. Auzel, P. Goldner, Opt. Mater. 16 (2001) 93.
[8] Y. Jestin, C. Armellini, A. Chiappini, A. Chiasera, M. Ferrari, C. Goyes, M. Montagna, E. Moser, G. Nunzi Conti, S. Pelli, R. Retoux, G.C. Righini, G. Speranza, J. Non-Cryst. Solids 353 (2007) 494.
[9] Y. Jestin, C. Armellini, A. Chiasera, A. Chiappini, M. Ferrari, E. Moser, R. Retoux, G.C. Righini, Appl. Phys. Lett. 91 (2007) 071909.
[10] G.C. Righini, M. Brenci, A. Chiasera, P. Feron, M. Ferrari, G. Nunzi Conti, S. Pelli, SPIE 6029 (2006) 19.
[11] R.R. Gonçalves, G. Carturan, L. Zampedri, M. Ferrari, M. Montagna, A. Chiasera, G.C. Righini, S. Pelli, S.J.L. Ribeiro, Y. Messaddeq, Appl. Phys. Lett. 81 (2002) 28.
[12] R.R. Gonçalves, G. Carturan, L. Zampedri, M. Ferrari, C. Armellini, A. Chiasera, M. Mattarelli, E. Moser, M. Montagna, G.C. Righini, S. Pelli, G. Nunzi Conti, S.J.L. Ribeiro, Y. Messaddeq, A. Minotti, V. Foglietti, H. Portales, SPIE 4990 (2003) 111.
[13] D.A. Neumayer, E. Cartier, J. Appl. Phys. 90 (2001) 1801.
[14] P. Myslinski, D. Nguyen, J. Chrostowski, J. Lightwave Technol. 15 (1997) 112.
[15] X. Orignac, D. Barbier, X.M. Du, R.M. Almeida, O. McCarty, E. Yeatman, Opt. Mater. 12 (1999) 1.
[16] L. Zampedri, C. Tosello, F. Rossi, S. Ronchin, R. Rolli, M. Montagna, A. Chiasera, G.C. Righini, S. Pelli, A. Monteil, S. Chaussedent, C. Bernard, C. Duverger, M. Ferrari, C. Armellini, SPIE 4282 (2001) 200.
[17] M.A. Krebs, R.A. Condrate, J. Am. Ceram. Soc. 65 (1982) C144.
[18] Y. Jestin, N.D. Afify, C. Armellini, S. Berneschi, S.N.B. Bhatka, B. Boulard, A. Chiappini, A. Chiasera, G. Dalba, C. Duverger, M. Ferrari, C.E. Goyes Lopez, M.

Mattarelli, M. Montagna, E. Moser, G. Nunzi Conti, S. Pelli, G.C. Righini, F. Rocca, SPIE 6183 (2006) 438.
[19] M. Ferrari, C. Armellini, S. Berneschi, M. Brenci, A. Chiappini, A. Chiasera, Y. Jestin, M. Mattarelli, M. Montagna, E. Moser, G. Nunzi Conti, S. Pelli, G.C. Righini, C. Tosello, SPIE 6183 (2006) 181.
[20] R.D. Robinson, J. Tang, M.L. Steigerwald, L.E. Brus, I.P. Herman, Phys. Rev. B 71 (2005) 115408.
[21] M. Montagna, E. Moser, F. Visintainer, M. Ferrari, L. Zampedri, A. Martucci, M. Guglielmi, M. Ivanda, J. Sol. Gel. Sci. Tech. 26 (2003) 241.
[22] W.C. Liu, D. Wu, A.D. Li, H.Q. Ling, Y.F. Tang, N.B. Ming, Appl. Surf. Sci. 191 (2002) 181.
[23] P.G. Kik, A. Polman, MRS Bull. 23 (1998) 48.
[24] V.S. Saridoghdar, F. Treussart, J. Hare, V. Lefèvre-Seguin, J.M. Raimond, S. Haroche, Phys. Rev. A 54 (1996) 1777.
[25] F. Lissillour, P. Féron, N. Dubreuil, P. Dupriez, M. Poulain, G. Stéphan, Elect. Lett. 36 (2000) 1382.
[26] M. Cai, O. Painter, K.J. Vahala, P.C. Sercel, Opt. Lett. 25 (2000) 1430.
[27] F. Lissillour, D. Messager, G.M. Stéphan, P. Féron, Opt. Lett. 26 (2001) 1051.
[28] Y. Jestin, C. Armellini, A. Chiappini, A. Chiasera, Y. Dumeige, M. Ferrari, P. Féron, L. Ghisa, G. Nunzi Conti, S. Trebaol, G.C. Righini, SPIE 6890 (2008) 689008-1.
[29] C. Arnaud, Phd Thesis, Université de Rennes I, 2004.
[30] Z.P. Cai, A. Chardon, H.Y. Xu, P. Féron, G. Stéphan, Opt. Commun. 203 (2002) 301.
[31] G.M. Stéphan, H.Y. Xu, Z.P. Cai, P. Féron, M. Mortier, SPIE 4629 (2002) 181.
[32] C. Arnaud, M. Boustimi, P. Féron, G. Nunzi-Conti, G. Righini, SPIE 5333 (2004) 140.
[33] Z.P. Cai, H.Y. Xu, G. Stéphan, P. Féron, M. Mortier, Opt. Commun. 229 (2004) 311.
[34] C. Arnaud, M. Boustimi, M. Brenci, Féron, M. Ferrari, G. Nunzi Conti, S. Pelli, G. Righini, SPIE 5622 (2004) 315.